Empirical Modeling of a Solar-Powered Energy Harvesting Wireless Sensor Node for Time-Slotted Operation

Pius Lee*, Zhi Ang Eu†, Mingding Han*, and Hwee-Pink Tan*
*Networking Protocols Department, Institute for Infocomm Research (I²R), A*STAR, Singapore
†NUS Graduate School for Integrative Sciences and Engineering, National University of Singapore
Email: {wqplee,mhan,hptan}@i2r.a-star.edu.sg and euzhiang@nus.edu.sg

***Abstract*—Energy harvesting wireless sensor networks (EH-WSNs) are gaining importance in smart homes, environmental monitoring, health care and transportation systems, since they enable much longer operation time as energy can be replenished through energy harvesting. This is unlike WSN nodes that use non-rechargeable batteries which need to be replaced once energy is depleted. However, the sporadic availability of ambient energy makes the design of networking protocols and predicting network performance very challenging. In this paper, we perform an empirical energy characterization of a time-slotted solar energy harvesting node with different system and environmental parameters. We use six different statistical models (uniform distribution, geometric distribution, transformed geometric distribution, Poisson distribution, transformed Poisson distribution and a Markovian model) to fit the empirical datasets. Our results show that there is no single statistical model that can fit all the datasets, thus justifying the need to use empirical data to validate the theoretical analysis of any time-slotted MAC protocol for EH-WSNs.**

I. Introduction

In traditional wireless sensor networks (WSNs), the stored energy in non-rechargeable batteries is used to operate the nodes and determines the network lifetime since it depletes with time. However, recent advances in energy harvesting technologies [1] have made it possible for low-power electronics such as wireless sensor nodes to be powered solely by ambient energy harvesting. Since harvesting rates achievable today still fall short of typical power consumption levels in wireless sensor nodes, the harvested energy may need to be accumulated in storage devices (e.g., capacitors, supercapacitors or thin-film batteries) to a sufficient level to operate the nodes.

Such energy harvesting wireless sensor networks (EH-WSNs) present an attractive alternative to traditional WSNs powered by non-renewable energy sources such as batteries due to the availability of different sources of ambient energy as well as the large number of recharge cycles (>tens of thousands) achievable by storage devices such as supercapacitors. For example, Mide, Microstrain, Micropelt, Enocean, AdaptivEnergy and Powercast have produced commercial energy harvesters that can convert ambient energy such as solar energy from light sources, vibrational energy from machinery, thermal energy from heat sources, mechanical energy from movement and RF energy from radio waves into electrical energy to power sensor nodes.

However, the expected high variability in the energy harvesting process, in both time and space, has exemplified the challenges in designing networking protocols [2] for EH-WSNs. In particular, it is important to obtain an accurate model of this process, and use this to drive the design of networking protocols. However, most of the data-sheets provided for commercial energy harvesters only describe the technology, mechanism and average rate of energy harvesting, while excluding important characteristics such as the time varying behavior of energy harvesting.

Many performance studies on EH-WSNs have assumed the use of a time-slotted system (e.g., [3]) with different energy harvesting models. In [3], it is assumed that the energy harvested in each slot is identical and independently distributed. In [4], the energy harvesting process is assumed to be deterministic while in [5], [6] and [7], the harvested energy is described using a Markovian model. In [8], we have carried out an empirical study to characterize the radio link as well as the energy harvesting characteristics of solar powered energy harvesting nodes to support our design, and evaluate the performance, of an asynchronous (non time-slotted) polling-based MAC protocol [9] for EH-WSNs.

In this paper, we extend our previous study to perform empirical modeling of a solar-powered EH-WSN node for time-slotted operation. Referring to Fig. 1, the output voltage of the energy storage device is sampled every t_s seconds, at the beginning of each time slot. The EH-WSN node can transmit a packet as long as the output voltage exceeds a certain operating voltage, V_o. Various operating and environmental parameters such as the transmit power, P_{tx}, the illuminance, I, as well as the time slot size, t_s, impact the time/space characteristics of the stored energy, i.e., the energy model.

To quantify the validity of various statistical energy models used in previous studies, we carried out extensive empirical measurements (i) using different slot sizes, t_s; (ii) under different light intensity levels, I, in indoor and outdoor environments; (iii) using different transmit power levels, P_{tx}, to characterize the energy model for a solar-powered energy harvesting node for time-slotted operation. Then, we apply well-known statistical models to fit the empirical data, and establish the goodness-of-fit of each model.

This paper is organized as follows: In Section II, we

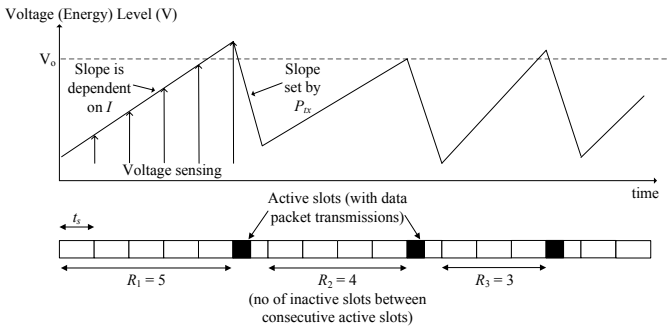

Fig. 1. Time Variation of Stored Energy in a EH-WSN node

describe the experimental setup. In Section III, we derive the parameters and probability distributions of well-known statistical models to our collected data. Then, we present and discuss the measurement results in Section IV. Finally, we conclude the paper and outline our future work in Section V.

II. Experimental Setup

The solar-powered EH-WSN platform that we use in this study is the Texas Instruments eZ430-RF2500-SEH platform [10], as shown in Fig. 2. Each platform consists of a target board, eZ430-RF2500T, as well as a SEH-01-DK solar energy harvesting board. The target board comprises a MSP430 microcontroller, an on-board antenna and a CC2500 radio transceiver [11] that operates in the 2.4 GHz band with data rate of 250 kbps. The transceiver is designed for low-power wireless applications and supports many transmit power levels (P_{tx}); Table I lists the corresponding current consumption for various P_{tx}. The solar energy harvesting board comprises a solar panel and energy management electronics, where the harvested energy is stored in thin-film EnerChip manufactured by Cymbet. Compared to normal batteries, the thin-film EnerChip is rechargeable and has little self-discharge, making it suitable for use in an EH-WSN node.

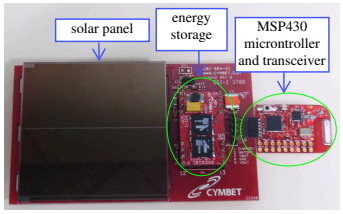

Fig. 2. The eZ430-RF2500-SEH Solar-Powered EH-WSN Platform

Each experimental setup comprises an eZ430-RF2500-SEH platform configured as the transmitter, and a target board configured as the receiver which is connected to (and powered) by a laptop for data logging. Referring to Fig. 1, at the beginning of each time slot, the microcontroller would be turned on and the node will check its voltage (which consumes a very small amount of energy). If the measured voltage exceeds the operating voltage, V_o (set to 3V in this study [10]), the transceiver will be switched on and a packet of size

TABLE I
Transceiver Current Consumption at Various Transmit Power Levels

Transmit Power, P_{tx} (dBm)	Current Consumption (mA)
-22	10.0
-10	12.2
-8	14.1
-4	16.2
-2	17.7
0	21.2

40 bytes (with 11 bytes of physical layer overheads) will be transmitted. Then, the transceiver and microcontroller would be switched off until the start of the next time slot and the entire process is repeated. Both the transmitter and receiver are placed very close together, so that transmission losses can be assumed to be negligible.

The time-slotted energy model in an EH-WSN node can be characterized empirically by measuring R_i, which denotes the number of inactive slots (where packet transmissions are not possible) between the i^{th} and $(i+1)^{th}$ data packet transmissions. After n_r measurements (set to 1,000 in this paper) are collected, the average transmission rate, α, in packets per second, can be computed as:

$$\alpha = \frac{n_r}{n_r + \sum_{i=1}^{n_r} R_i} \left(\frac{1}{t_s}\right) \quad (1)$$

We repeat the above measurements by varying various system and environmental parameters including the slot size, light intensity, power level and the type of environment: (i) t_s is varied from 5 ms to 1 second; (ii) indoor light intensity, I, is varied by placing the transmitter at different distances from a desk fluorescent lamp (Fig. 3a) in our indoor lab; (iii) outdoor light intensity, I, is varied by deploying the setup in an outdoor carpark as shown in Fig. 3b at various times of the day; and (iv) P_{tx} is varied according to Table I.

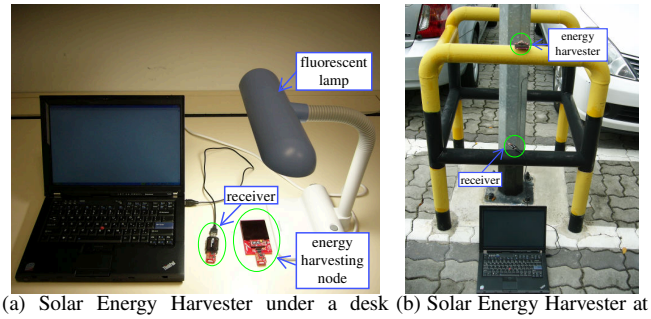

(a) Solar Energy Harvester under a desk fluorescent lamp (b) Solar Energy Harvester at an outdoor carpark

Fig. 3. Placement of solar-powered EH-WSN node for energy measurements

III. Statistical Energy Models for Time-Slotted EH-WSN

In this section, we describe various statistical models that we will use to fit the measurements, $\{R_i\}_{i=1}^{n_r}$, obtained from the experiments described in Section II. These models include the discrete uniform distribution, the geometric distribution, the Poisson distribution and a two-state Markovian model.

A. Discrete uniform distribution

In the discrete uniform distribution (**UD**), the random variable R assumes each of its value with equal probabilities. We let R_{min} and R_{max} be the minimum and maximum value of the collected values (R_1 to R_{n_r}) in each scenario. The distribution of R is given by

$$P(R = x) = \frac{1}{R_{max} - R_{min} + 1}, \tag{2}$$

where $x \in [R_{min}, R_{min} + 1, ..., R_{max}]$.

B. Geometric distribution

In the geometric distribution (**GD**), the random variable R is defined as the number of inactive slots before a data transmission can take place. The probability of transmission in a slot, p_{GD}, is given by:

$$p_{GD} = \frac{n_r}{n_r + \sum_{i=1}^{n_r} R_i}, \tag{3}$$

and the distribution of R is given by

$$P(R = x) = (1 - p_{GD})^x p_{GD}, \tag{4}$$

where $x \in [0, 1, 2, ..., \infty)$.

C. Transformed Geometric distribution

In some scenarios, the fitting can be improved by doing some transformation to the data before using the geometric distribution. For example, we can use the following transformation $S_i = R_i - R_{min}$. We denote this distribution as the transformed geometric distribution (**TGD**). The corresponding probability of transmission, p_{TGD}, is given by:

$$p_{TGD} = \frac{n_r}{n_r + \sum_{i=1}^{n_r} S_i}, \tag{5}$$

and the distribution of R is given by

$$\begin{aligned} P(R = x) &= P(S = x - R_{min}) \\ &= (1 - p_{TGD})^{x - R_{min}} p_{TGD}, \end{aligned} \tag{6}$$

where $x \in [R_{min}, R_{min} + 1, ..., \infty)$.

D. Poisson distribution

In the Poisson distribution (**PD**), the sample average of the measured R values is given by $R_{avg} = \frac{\sum_{i=1}^{n_r} R_i}{n_r}$. Accordingly, the distribution of R is given by

$$P(R = x) = \frac{e^{-R_{avg}} {R_{avg}}^x}{x!}, \tag{7}$$

where $x \in [0, 1, 2, ..., \infty)$.

E. Transformed Poisson distribution

Similar to the geometric distribution, it is possible to improve the fitting to the Poisson distribution by using the transformation $S_i = R_i - R_{min}$. We denote this distribution as the transformed Poisson distribution (**TPD**). We denote the sample average of the measured S values by $S_{avg} = \frac{\sum_{i=1}^{n_r} S_i}{n_r}$. The distribution of R is then given by

$$\begin{aligned} P(R = x) &= P(S = x - R_{min}) \\ &= \frac{e^{-S_{avg}} {S_{avg}}^{(x - R_{min})}}{(x - R_{min})!} \end{aligned} \tag{8}$$

where $x \in [R_{min}, R_{min} + 1, ..., \infty)$.

F. Markovian model

Finally, we consider a two-state Markovian model (**MM**) in this paper as illustrated in Fig. 4 with the transition probabilities (p_{00}, p_{01}, p_{10} and p_{11}) calculated from each empirical dataset. In each time slot, the node will be in one of the two states: in the "0" state, the node cannot transmit a data packet as there is insufficient energy harvested while in the "1" state, the node can transmit a data packet.

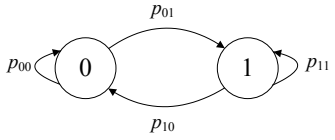

Fig. 4. Two-state Markovian model

The distribution of R is given by

$$P(R = x) = \begin{cases} p_{11}, & x = 0 \\ p_{10} * {p_{00}}^{x-1} * p_{01}, & x = 1, 2, ..., \infty \end{cases} \tag{9}$$

For each statistical model, **X**, we use a chi-square goodness-of-fit test with a 95% confidence interval to determine if it fits the empirical datasets, and denote a successful fit by **X(F)**. If there is no successful fit for all the six statistical distributions, we denote the nearest fit, **Y** (with the lowest chi-square value) by **Y(NF)**.

IV. Results and Discussion

In this section, we illustrate the results for the transmission rate as well as distribution fitting for each dataset. To illustrate the time variability of solar energy harvesting, we first placed the transmitter under a desk fluorescent lamp with a constant light intensity of 1,000 lux (measured by using a lux meter) with transmission power of 0 dBm. Fig. 5 shows the number of inactive slots required to harvest enough energy for the i^{th} data packet before it can be transmitted. The results show that the harvesting time exhibits significant variation in time even in the absence of mobility and under controlled illuminance.

Next, we fit the six different statistical models to the dataset collected for the above scenario, and the results are shown in Fig. 6. There is no suitable fit using the chi-square test but the transformed Poisson distribution gives the nearest fit with the lowest chi-square value.

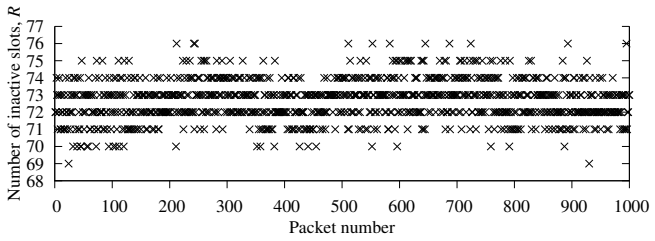

Fig. 5. Time variation of indoor light energy harvesting (P_{tx} = 0 dBm, I = 1,000 lux)

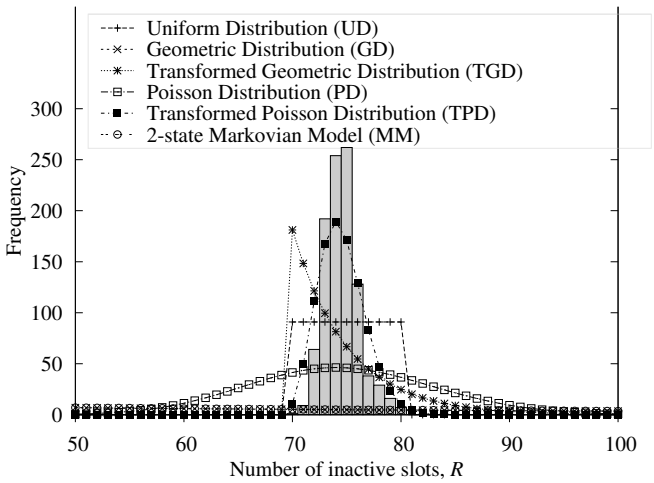

Fig. 6. Illustration of goodness-of-fit obtained with various statistical models (P_{tx} = 0 dBm, I = 1,000 lux) with **TPD(NF)**

A. Stored energy characteristics vs time slot duration (P_{tx}=0 dBm, I=1,000 lux)

Fig. 7 shows the variation of average transmission rate with the time slot duration for the indoor environment, with P_{tx} = 0 dBm, and I = 1,000 lux. When t_s is sufficiently high (i.e., 0.5 to 1 sec), the number of inactive slots is 0 since sufficient energy is harvested at the beginning of each slot, and thus, we can increase the sending rate by reducing t_s. The maximum sending rate is obtained by setting t_s to 0.1 second. Below that, the sending rate is reduced since measuring the voltage at the start of each time slot would require a small amount of energy, therefore reducing the slot duration would increase the voltage sampling rate, thereby decreasing the available amount of harvested energy for sending data packets.

Fig. 8 shows the best distribution fit for each dataset obtained at various t_s. Since R = 0 for t_s = 0.5 and 1, there is no statistical fit for these values. For t_s = 0.2, the Markovian model fits the empirical data perfectly while for the other values of t_s, there is no statistical distribution that fits, with the transformed Poisson distribution having the nearest fit.

B. Stored energy characteristics vs illuminance (P_{tx}=0 dBm, t_s=5 ms)

Next, we fixed the time slot duration to 5 ms and vary the light intensity by changing the distance between the transmitter and the desk fluorescent lamp, and the corresponding results

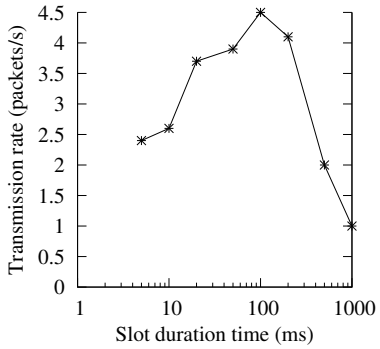

Fig. 7. Average transmission rate (α) for various time slot durations

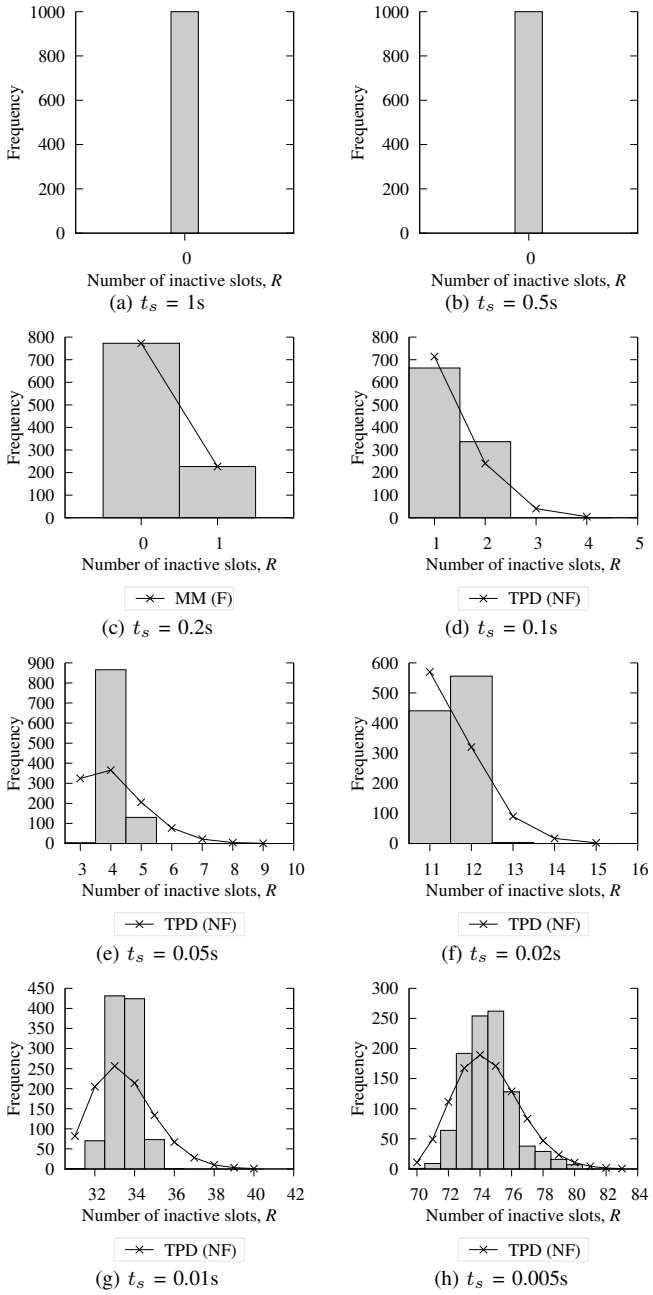

Fig. 8. Best-fitting statistical model obtained for various time slot durations

are plotted in Figs. 9 and 10. When the light intensity increases, the transmission rate increases while the average number of inactive time slots decreases. In this scenario, the transformed Poisson distribution has the nearest fit for all the datasets.

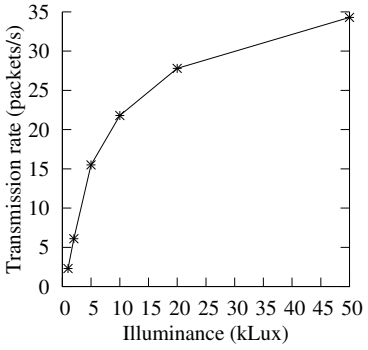

Fig. 9. Average transmission rate (α) for different light intensity

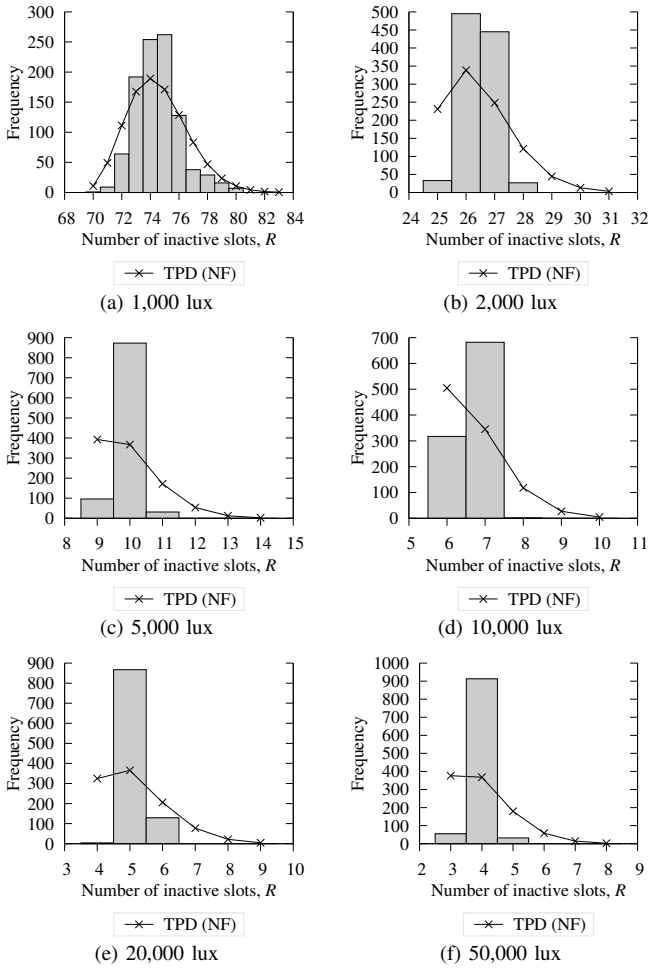

(a) 1,000 lux (b) 2,000 lux

(c) 5,000 lux (d) 10,000 lux

(e) 20,000 lux (f) 50,000 lux

Fig. 10. Energy harvesting characteristics for different light intensity

C. Stored energy characteristics vs transmission power (I=1,000 lux, t_s=5 ms)

Next, for the same indoor scenario, we vary the transmit power while keeping the light intensity constant at 1,000 lux and t_s = 5 ms, and plot the corresponding results in Figs. 11 and 12. As the transmit power increases, the average number of transmission decreases because the energy required to send a data packet increases. All the datasets in this scenario have the transformed Poisson distribution as the nearest fit.

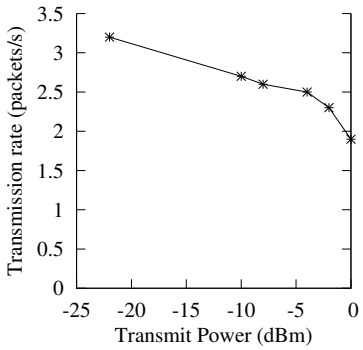

Fig. 11. Average transmission rate (α) for different transmit powers

D. Stored energy characteristics in outdoor environment (P_{tx}= 0 dBm, t_s=5 ms)

Finally, we placed the experimental setup in an outdoor carpark and repeated the measurements at different times of the day (from 0800 to 1800 hrs). The transmit power is set to 0 dBm, and the time slot duration is set to 5 ms. The corresponding results are plotted in Figs. 13 and 14. As expected, the energy harvesting rate increases as we approach noon, when the sun is the strongest, but decreases towards the evening, when the sun begins to set. For this scenario, the uniform distribution has the nearest fit for two datasets while the transformed Poisson distribution has the nearest fit for four datasets.

V. Conclusion and Future Work

In this paper, we have carried out extensive measurements for empirical modeling of a solar-energy powered wireless sensor node for time-slotted operation. Our empirical measurements show that the stored energy characteristics depend on many factors including the time slot duration, light intensity, power level as well as the deployment environment. We also evaluated the goodness-of-fit of six statistical models to the collected measurements. Our results show that the transformed Poisson distribution achieves the nearest fit for most datasets, while the two-state Markovian model achieves a successful fit only for one particular data set. This illustrates the need to validate analytical results from theoretical analysis with empirical measurements, as well as the need for better statistical models that may achieve more accurate fitting.

For future work, we are planning to extend our measurements to other type of energy harvesters including thermal

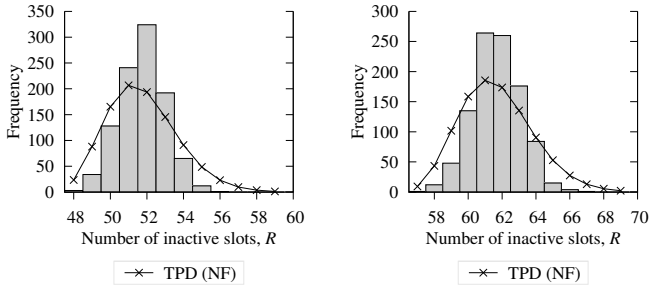

(a) -22 dBm

(b) -10 dBm

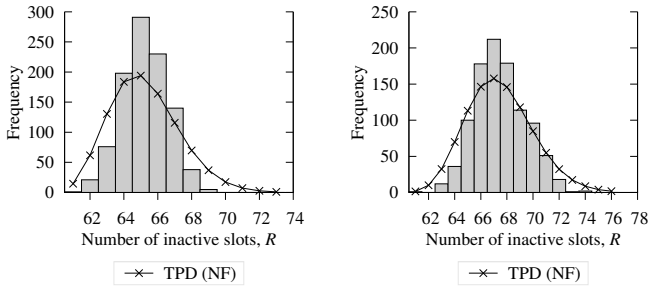

(c) -8 dBm

(d) -4 dBm

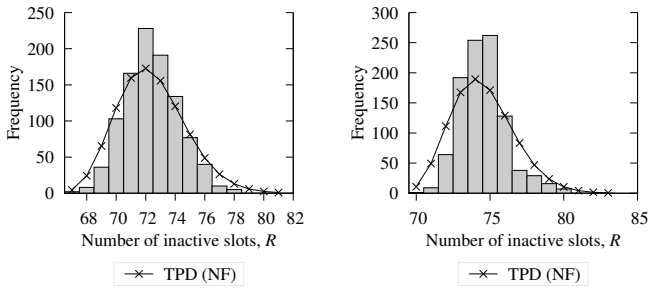

(e) -2 dBm

(f) 0 dBm

Fig. 12. Energy harvesting characteristics for different transmit powers

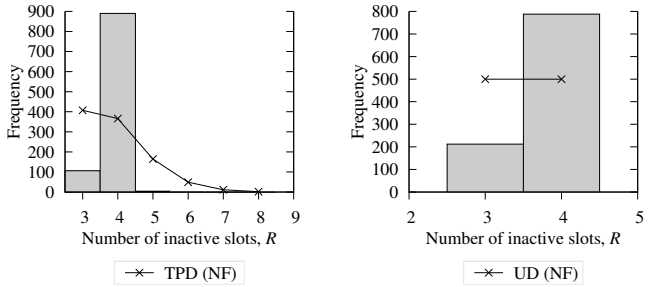

(a) 8am (35,000 lux)

(b) 10am (48,000 lux)

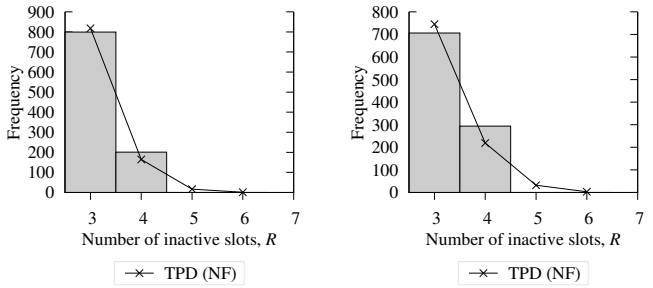

(c) 12noon (130,000 lux)

(d) 2pm (110,000 lux)

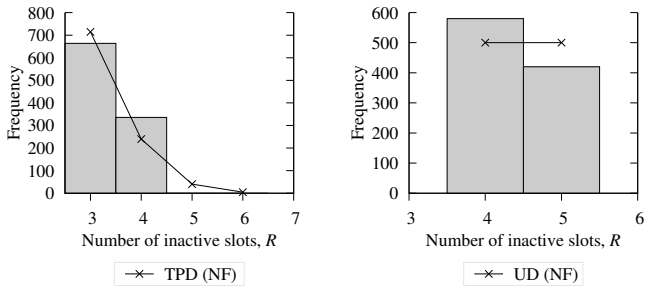

(e) 4pm (82,000 lux)

(f) 6pm (24,000 lux)

Fig. 14. Energy harvesting characteristics at different time of the day

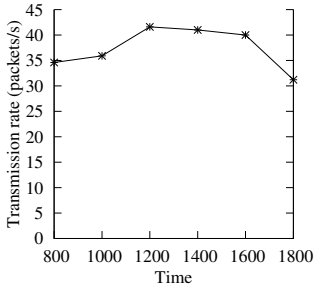

Fig. 13. Average transmission rate (α) at different time of the day

and vibrational energy harvesters. Furthermore, we are also investigating other statistical models to improve the modeling accuracy of the energy harvesting process.

REFERENCES

[1] J. A. Paradiso and T. Starner, "Energy Scavenging for Mobile and Wireless Electronics," *IEEE Pervasive Computing*, vol. 4, no. 1, pp. 18–27, 2005.

[2] S. Sudevalayam and P. Kulkarni, "Energy Harvesting Sensor Nodes: Survey and Implications," *IEEE Commun. Surveys Tuts.*, 2010.

[3] B. Medepally, N. B. Mehta, and C. R. Murthy, "Implications of Energy Profile and Storage on Energy Harvesting Sensor Link Performance," in *Globecom*, 2009.

[4] M. Tacca, P. Monti, and A. Fumagalli, "Cooperative and Reliable ARQ Protocols for Energy Harvesting Wireless Sensor Nodes," *IEEE Trans. Wireless Commun.*, vol. 6, no. 7, pp. 2519–2529, Jul 2007.

[5] A. Seyedi and B. Sikdar, "Energy Efficient Transmission Strategies for Body Sensor Networks with Energy Harvesting," *IEEE Trans. Commun.*, vol. 58, no. 7, pp. 2116–2126, Jul 2010.

[6] J. Lei, R. Yates, and L. Greenstein, "A Generic Model for Optimizing Single-Hop Transmission Policy of Replenishable Sensors," *IEEE Trans. Wireless Commun.*, vol. 8, no. 2, pp. 547–551, Feb. 2009.

[7] C. K. Ho and R. Zhang, "Optimal Energy Allocation for Wireless Communications Powered by Energy Harvesters," in *IEEE International Symposium on Information Theory*, 2010.

[8] Z. A. Eu, H. P. Tan, and W. K. G. Seah, "Wireless Sensor Networks Powered by Ambient Energy Harvesting: An Empirical Characterization," in *IEEE International Conference on Communications (ICC)*, 2010.

[9] Z. A. Eu, H.-P. Tan, and W. K. G. Seah, "Design and Performance of MAC Schemes for Wireless Sensor Networks Powered by Ambient Energy Harvesting," *to appear in Ad Hoc Networks*, 2010.

[10] "MSP430 Solar Energy Harvesting Development Tool (eZ430-RF2500-SEH) from Texas Instruments." [Online]. Available: http://www.ti.com

[11] CC2500 Datasheet, "Low-Cost Low-Power 2.4 GHz RF Transceiver." [Online]. Available: http://focus.ti.com/docs/prod/folders/print/cc2500.html